THE EFFECT OF CURVATURE ON THE TRANSITION TO TURBULENCE IN CIRCULAR PIPES

By
ADDISON GUY HARDEE, JR.

A THESIS PRESENTED TO THE GRADUATE COUNCIL OF
THE UNIVERSITY OF FLORIDA
IN PARTIAL FULFILLMENT OF THE REQUIREMENTS FOR THE
DEGREE OF MASTER OF SCIENCE IN ENGINEERING

UNIVERSITY OF FLORIDA
December, 1965

ACKNOWLEDGMENTS

The author wishes to express his sincerest appreciation to his supervisory committee for their cooperation and efforts, and in particular to Drs. K. T. Millsaps and M. H. Clarkson.

Appreciation is also expressed to Dr. R. L. Fearn for his kind assistance and to E. C. Logsdon for his expert fabrication of the glass-work so necessary to the investigation.

Further appreciation is expressed to the National Aeronautics and Space Administration for financial support extended through a fellowship and to the Air Force Office of Scientific Research for grant AF-AFOSR-842-65 which has made the continuation of this research possible.

TABLE OF CONTENTS

Page

ACKNOWLEDGMENTS ii

LIST OF FIGURES iv

LIST OF SYMBOLS v

ABSTRACT vii

CHAPTERS

I INTRODUCTION 1
  1. Scope 1
  2. Experimental Investigations Concerning Transition in Curved Pipes 1
  3. The Electric Double Layer 22
  4. Streaming Potential 26
  5. Results of Anderson's Investigation 28

II THE EXPERIMENT 29
  1. General Description 29
  2. Laboratory 29
  3. Apparatus 30
  4. Curving and Measuring of the Glass Pipes 37
  5. Experimental Procedures 37

III RESULTS 41
  1. Measurements 41

APPENDIX I 44

BIBLIOGRAPHY 47

LIST OF FIGURES

Figure		Page
1.	Dean's coordinate system for flow in a curved pipe.	4
2.	Model showing Dean's velocity profiles of flow in a curved pipe.	13
3.	Dean's streamlines in the plane of the pipe's cross section.	15
4.	Results of White's experiments showing resistance coefficient vs. Dean's similarity parameter.	18
5.	Schematic representation of Taylor's color band which described the general type of motion found analytically by Dean for laminar flow.	21
6.	Reproduction of Taylor's fig. 3.	24
7.	Schematic sketch of experimental apparatus.	32
8.	A sketch of the pressure system.	34
9.	Manometer and optical system used for the pressure measurements.	36
10.	Tube calibration curve.	40
11.	Critical Reynolds number vs. curvature ratio.	43

LIST OF SYMBOLS

a	radius of pipe bore
e	electronic charge
E	streaming potential
G	mean pressure gradient
h	scale factor
i_1	electrical convection current
K	similarity parameter
K'	similarity parameter, Goldstein's form
K'_D	similarity parameter, Dean's form
n_i	number density of the ith ion species
p	pressure
r	coordinate measured from center of pipe
r'	nondimensional form of r
R	radius of curvature of pipe
s	arc length
T	temperature
U	velocity in the r direction
V	velocity in the Ψ direction
W	velocity in the θ direction
W_0	mean velocity of the flow through a straight pipe
W_m	mean velocity along center line of pipe
x	Cartesian coordinate
X	reciprocal of Debye length

y	Cartesian coordinate
z	Cartesian coordinate
ϵ	dielectric constant
θ	polar coordinate
κ	Boltzmann constant
λ	specific conductance
μ	viscosity
ν	kinematic viscosity
ζ	potential in the electric double layer
ρ	fluid density
τ_0	shearing stress at wall
ϕ	nondimensional stream function
ψ	polar coordinate

Abstract of Thesis Presented to the Graduate Council
in Partial Fulfillment of the Requirements for the
Degree of Master of Science in Engineering

THE EFFECT OF CURVATURE ON THE TRANSITION TO TURBULENCE IN CIRCULAR PIPES

By

Addison Guy Hardee, Jr.

December, 1965

Chairman: Dr. K. T. Millsaps
Major Department: Aerospace Engineering

The experimental determination of the critical Reynolds number for transition from laminar to turbulent flow in a curved pipe of circular cross section has been accomplished by the use of a streaming potential technique. The streaming potential was generated by an electrolyte (0.001 M KCl) flowing through a capillary tube with a diameter of 0.0709 inches with a radius of curvature of 55.9 inches. At the onset of turbulence, the streaming potential began to fluctuate in an early identifiable manner. This fluctuation, combined with mass flow measurements, was used to determine the critical Reynolds number to be 3190 ± 10 for a fixed geometry and fluid.

I. INTRODUCTION

1. Scope

The purpose of the present investigation is to determine the effect of curvature on the transition from laminar to turbulent flow in pipes of circular cross section. The technique used in observing the onset of turbulence is one developed by Anderson(1) involving the electric double layer.

2. Experimental Investigations Concerning Transition in Curved Pipes

The experimental investigations of flow in curved pipes may be divided into two main classes: those prior to a paper by Dean(2), and those following. Dean showed from a mathematical analysis of the equations of motion that dynamical similarity depends only on the parameter

$$K'_D = \left(\frac{a}{R}\right)\left(\frac{2W_o^2 a^2}{\nu^2}\right) \tag{1}$$

where a is the radius of the pipe bore,

R is the radius of curvature of the pipe,

W_o is the mean velocity of the flow through a straight pipe under the same pressure gradient,

and ν is the kinematic viscosity of the fluid.

Of course, dimensional analysis shows that any dynamical quantity depends on the functional form $f_1\left(\frac{a}{R}, \frac{W_0 a}{\nu}\right)$, where $\frac{W_0 a}{\nu}$ is a Reynolds number. A particularly simple form is $\frac{W_0 a^2}{R \nu}$.

To do this Dean considered the flow of an incompressible fluid in the coordinate system where (r, ψ, θ) are the orthogonal coordinates (specified in Fig. 1). The corresponding velocity components are (U,V,W) respectively. It is assumed that the flow is steady and that U,V and W , but not the pressure, are independent of θ .

The general orthogonal curvilinear form of the Navier-Stokes equations and the continuity equation are given for reference in Appendix I. In the transformation to Dean's coordinate system

$$l = R + r \sin \psi \tag{2}$$

$$\begin{aligned} x &= l \cos \theta = (R + r \sin \psi) \cos \theta \\ y &= l \sin \theta = (R + r \sin \psi) \sin \theta \\ z &= r \cos \theta \end{aligned} \tag{3}$$

Fig. 1. Dean's coordinate system for flow in a curved pipe.

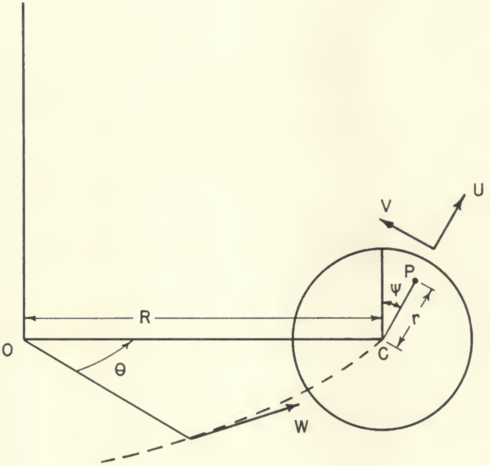
U
V
P
Ψ
R
r
O
C
θ
W

and therefore the scale factors are

$$h_1 = \sqrt{\left(\frac{\partial x}{\partial r}\right)^2 + \left(\frac{\partial y}{\partial r}\right)^2 + \left(\frac{\partial z}{\partial r}\right)^2}$$

$$h_2 = \sqrt{\left(\frac{\partial x}{\partial \psi}\right)^2 + \left(\frac{\partial y}{\partial \psi}\right)^2 + \left(\frac{\partial z}{\partial \psi}\right)^2} \qquad (4)$$

$$h_3 = \sqrt{\left(\frac{\partial x}{\partial \theta}\right)^2 + \left(\frac{\partial y}{\partial \theta}\right)^2 + \left(\frac{\partial z}{\partial \theta}\right)^2}$$

Thus to write the Navier-Stokes equations of motion for Dean's coordinate system we use the relations

$$\begin{aligned} \chi_1 &= r \ , & \omega_1 &= U \\ \chi_2 &= \psi \ , & \omega_2 &= V \\ \chi_3 &= \theta \ , & \omega_3 &= W \end{aligned} \qquad (5)$$

$$\begin{aligned} h_1 &= 1 \\ h_2 &= r \\ h_3 &= R + r\sin\theta \end{aligned} \qquad (6)$$

The continuity equation becomes

$$\frac{\partial U}{\partial r} + \frac{U}{r} + \frac{U\sin\psi}{R + r\sin\psi} + \frac{1}{r}\frac{\partial V}{\partial \psi} + \frac{V\cos\psi}{R + r\sin\psi} = 0 \qquad (7)$$

Denoting the vector sum of the velocity components as $\bar{v}$ and since $\mathrm{div}\,\bar{v} = 0$, we may add the expression $B\frac{\partial}{\partial x_i}(\mathrm{div}\,\bar{v})$ (where B is any constant) to the Navier-Stokes equations. To the first equation of motion we add $2\nu\frac{\partial}{\partial r}(\mathrm{div}\,\bar{v})$, to the second, add $2\frac{\nu}{r}\frac{\partial}{\partial \psi}(\mathrm{div}\,\bar{v})$. Nothing is added to the third. The equations of motion are then

$$U\frac{\partial U}{\partial r} + \frac{V}{r}\frac{\partial U}{\partial \psi} - \frac{V^2}{r} - \frac{W^2 \sin\psi}{R + r\sin\psi} = -\frac{\partial}{\partial r}\left(\frac{p}{\rho}\right)$$

$$-\nu\left(\frac{1}{r}\frac{\partial}{\partial \psi} + \frac{\cos\psi}{R + r\sin\psi}\right)\left(\frac{\partial V}{\partial r} + \frac{V}{r} - \frac{1}{r}\frac{\partial U}{\partial \psi}\right) \qquad (8)$$

$$U\frac{\partial V}{\partial r} + \frac{V}{r}\frac{\partial V}{\partial \psi} + \frac{UV}{r} - \frac{W^2 \cos\psi}{R + r\sin\psi} = -\frac{1}{r}\frac{\partial}{\partial \psi}\left(\frac{p}{\rho}\right)$$

$$+\nu\left(\frac{\partial}{\partial r} + \frac{\sin\psi}{R + r\sin\psi}\right)\left(\frac{\partial V}{\partial r} + \frac{V}{r} - \frac{1}{r}\frac{\partial U}{\partial \psi}\right) \qquad (9)$$

and

$$U\frac{\partial W}{\partial r} + \frac{V}{r}\frac{\partial W}{\partial \psi} + \frac{UW\sin\psi}{R + r\sin\psi} + \frac{VW\cos\psi}{R + r\sin\psi}$$

$$= -\frac{1}{R + r\sin\psi}\frac{\partial}{\partial \theta}\left(\frac{p}{\rho}\right) + \nu\left[\left(\frac{\partial}{\partial r} + \frac{1}{r}\right)\left(\frac{\partial W}{\partial r} + \frac{W\sin\psi}{R + r\sin\psi}\right)\right.$$

$$\left. + \frac{1}{r}\frac{\partial}{\partial \psi}\left(\frac{1}{r}\frac{\partial W}{\partial \psi} + \frac{W\cos\psi}{R + r\sin\psi}\right)\right] \qquad (10)$$

With the assumption that $^a/_R$ is small, the equations of motion become

$$U\frac{\partial U}{\partial r} + \frac{V}{r}\frac{\partial U}{\partial \psi} - \frac{V^2}{r} - \frac{W^2 \sin\psi}{R}$$

$$= \frac{\partial}{\partial r}\left(\frac{p}{\rho}\right) - \frac{\nu}{r}\frac{\partial}{\partial \psi}\left(\frac{\partial V}{\partial r} + \frac{V}{r} - \frac{1}{r}\frac{\partial U}{\partial \psi}\right) \tag{11}$$

$$U\frac{\partial V}{\partial r} + \frac{V}{r}\frac{\partial V}{\partial \psi} + \frac{UV}{r} - \frac{W^2 \cos\psi}{R}$$

$$= \frac{1}{r}\frac{\partial}{\partial \psi}\left(\frac{p}{\rho}\right) + \nu\frac{\partial}{\partial r}\left(\frac{\partial V}{\partial r} + \frac{V}{r} - \frac{1}{r}\frac{\partial U}{\partial \psi}\right) \tag{12}$$

and

$$U\frac{\partial W}{\partial r} + \frac{V}{r}\frac{\partial W}{\partial \psi} = -\frac{1}{R}\frac{\partial}{\partial \theta}\left(\frac{p}{\rho}\right)$$

$$+ \nu\left(\frac{\partial^2 W}{\partial r^2} + \frac{1}{r}\frac{\partial W}{\partial r} + \frac{1}{r^2}\frac{\partial^2 W}{\partial \psi^2}\right) \tag{13}$$

and the continuity equation is

$$\frac{\partial U}{\partial r} + \frac{U}{r} + \frac{1}{r}\frac{\partial V}{\partial \psi} = 0 \tag{14}$$

Since U , V and W are assumed to be independent of Θ , then from (13) it may be seen that P/ρ must have the form

$$\Theta f_1(r, \psi) + f_2(r, \psi)$$

From (11) and (12) it may also be seen that f_1 must be a constant. Thus we can write

$$-\frac{1}{R}\frac{\partial}{\partial\Theta}\left(\frac{P}{\rho}\right) = \frac{G}{\rho} \tag{15}$$

where G is a constant and is the mean pressure gradient.

We may satisfy the continuity equation with

$$rU = -\frac{\partial f}{\partial\psi} \quad , \quad V = \frac{\partial f}{\partial r} \tag{16}$$

where $f = f(r, \psi)$. Using relations (16) in the equations of motion and eliminating p from (11) and (12), we have the two equations

$$\left(\frac{\partial f}{\partial\psi}\frac{\partial}{\partial r} - \frac{\partial f}{\partial r}\frac{\partial}{\partial\psi}\right)\nabla_1^2 f + \frac{2W}{R}\left(r\cos\psi\frac{\partial W}{\partial r} - \sin\psi\frac{\partial W}{\partial\psi}\right)$$

$$= -\nu r\nabla_1^4 f \tag{17}$$

and

$$\frac{1}{r}\left(\frac{\partial f}{\partial r}\frac{\partial W}{\partial \psi} - \frac{\partial f}{\partial \psi}\frac{\partial W}{\partial r}\right) = \frac{G}{\rho} + \nu \nabla_1^2 W \tag{18}$$

where

$$\nabla_1^2 \equiv \frac{\partial^2}{\partial r^2} + \frac{1}{r}\frac{\partial}{\partial r} + \frac{1}{r^2}\frac{\partial^2}{\partial \psi^2} \tag{19}$$

We may put equations (17) and (18) into non-dimensional form by using

$$f = \nu \phi \quad , \quad W = W_0 \omega \quad , \quad r = a r' \tag{20}$$

where W_0 has the dimensions of a velocity. The equations are then

$$\left(\frac{\partial \phi}{\partial \psi}\frac{\partial}{\partial r'} - \frac{\partial \phi}{\partial r'}\frac{\partial}{\partial \psi}\right)\nabla_1^2 \phi + K_D' \omega\left(r' \cos\psi \frac{\partial \omega}{\partial r'} - \sin\psi \frac{\partial \omega}{\partial \psi}\right)$$

$$= - r' \nabla_1^4 \phi \tag{21}$$

and

$$\frac{1}{r'}\left(\frac{\partial \phi}{\partial r'}\frac{\partial \omega}{\partial \psi} - \frac{\partial \phi}{\partial \psi}\frac{\partial \omega}{\partial r'}\right) = C + \nabla_1^2 \omega \tag{22}$$

where

$$K_D' = \frac{2W_0^2 a^3}{\nu^2 R} \quad , \qquad C = \frac{G a^2}{\mu W_0} \tag{23}$$

Now ∇_1^2 denotes the non-dimensional form of the operator. If the motion is slow W_0 may be considered to be the velocity component along the center of the pipe; thus $\frac{a W_0}{\nu}$ is approximately the Reynolds number. The boundary conditions to be satisfied are

$$\frac{\partial \Phi}{\partial r'} = \frac{\partial \Phi}{\partial \psi} = \omega = 0 \tag{24}$$

at $r' = 1$. Thus for laminar flow dynamical similarity depends solely on the parameter K_D' .

Using Goldstein's(3) notation,

$$K' = \left(\frac{a}{R}\right)^{1/2} \left(\frac{2 W_0 a}{\nu}\right) \tag{25}$$

This may be replaced, to a first approximation, by

$$K = \left(\frac{a}{R}\right)^{1/2} \left(\frac{2 W_m a}{\nu}\right) \tag{26}$$

where W_m is the mean velocity of the flow in the curved pipe. K is a function of K' alone since W_m/W_o is a function of K' alone, so that dynamical similarity depends on K . (Dean also gave the equations of the velocity profiles, and a model which shows the profiles has been constructed. See Figure 2 . The secondary flow resulting from the curvature is indicated by the streamlines in the plane of the cross section, shown in Fig. 3 .)

Investigations prior to Dean's work suffered from lack of a similarity parameter so that, though it was known that curvature of a pipe increased the resistance to flow above that of a straight pipe, the results of experiments were not as systematic as desired.

Experiments that are illustrative of these early investigations were: those of Grindley and Gibson(4), conducted to determine the viscosity of air; and those of Eustice(5), conducted to study the effects of curvature. The tests of Grindley and Gibson extended over the range of Reynolds numbers from 25 to 1400 and, hence, did not cover the transition to turbulence; also only one radius of curvature was studied. The tests of Eustice covered a wide range of Reynolds numbers (from 21 to 6000 for one pipe) and curvatures, but the pipes did not have a circular cross section. Also, no inlet length was provided for full flow development ahead of the testing length.

It had long been known that for flow in a straight pipe the resistance is proportional to the velocity of flow

Fig. 2. Model showing Dean's velocity profiles of flow in a curved pipe.

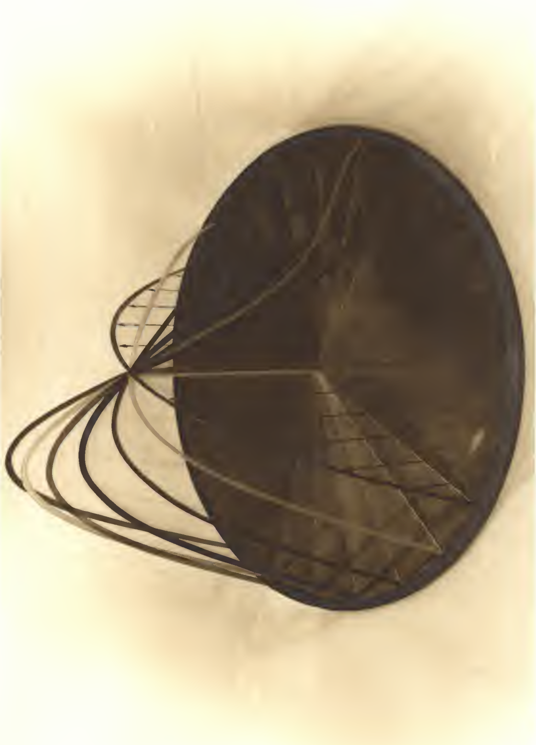

Fig. 3. Dean's streamlines in the plane of the pipe's cross section. The points denoted by x represent lines of zero velocity along the pipe.

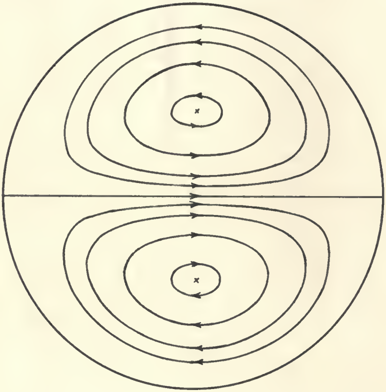

when the flow is laminar, but it ceases to be proportional at some velocity, which is known to be the critical velocity at which transition occurs. It was also known that curving a pipe caused the resistance to deviate from this proportionality at a lower velocity than that of the straight pipe. Early investigators thought this indicated that turbulence was established when this deviation occurred, so that flow in a curved pipe was considered to be less stable than that in a straight pipe.

Dean, however, stated that the secondary flow of the curved pipe, which is the cause of the increase in resistance, is a steady motion. Eustice seemed to think that there apparently was no critical velocity for flow in curved pipes. For the above lack of better experimental data, Dean seemed to accept Eustice's view.

Shortly after the publication of Dean's paper, White(6) conducted resistance measurements on pipes of three curvatures, and then he plotted his results together with those of Grindley and Gibson as a function of Dean's similarity parameter and apparently confirmed Dean's analysis. Furthermore, he correctly deduced from his graphical results that transition occurred when the curve for a particular curvature ratio left the main curve, i.e., ceased to be solely a function of Dean's parameter. The graph is reproduced as Figure 4 . For a curvature ratio of 1/2050 transition occurred at a Reynolds number of about 2300, while a ratio of 1/15.5 required a Reynolds number of about

Fig. 4. Results of White's experiments showing resistance coefficient vs. Dean's similarity parameter. White's actual data points are not reproduced.

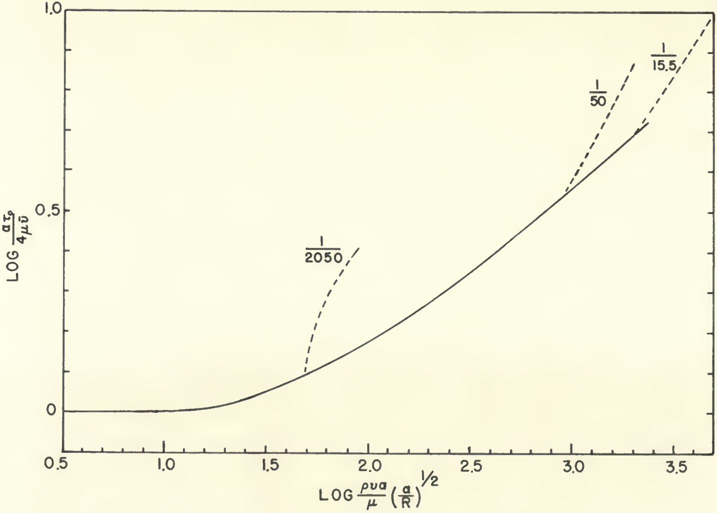

1.0
0.5
0
$\mathrm{LOG}\,\frac{a\tau_0}{4\mu\bar{v}}$
0.5
1.0
1.5
2.0
2.5
3.0
3.5
$\mathrm{LOG}\,\frac{\rho v a}{\mu}\left(\frac{a}{R}\right)^{1/2}$
$\frac{1}{2050}$
$\frac{1}{50}$
$\frac{1}{15.5}$

9000. Thus it appeared that the minimum critical Reynolds number for flow in a curved pipe depended on the curvature ratio.

That this was so was at once verified directly by Taylor(7) who injected a stream of dye into the flow in a helical pipe and observed the onset of turbulence visually. At the same time he confirmed Dean's analysis of the secondary flow which was traced out by Taylor's color band shown graphically in Figure 5. Taylor writes,

> As in Reynolds' experiments with a straight pipe, it was found that the flow was steady up to a certain speed. At this speed the colour band began to vibrate in an irregular manner, but it still seemed to retain its identity through at least one whole turn of the helix. This indicates that the unsteadiness was not at first of a type which gives rise to diffusion of momentum by eddies and hence to a rapid rise in resistance. In fig. 3, which shows graphically the results of these measurements, the point where this irregular vibration first made its appearance is indicated by a square, thus ▣ .
>
> On increasing the speed this irregular vibration increased in violence till, at a point which could be measured with some accuracy, the stream became completely turbulent so that the identity of the colour band was lost in a distance of a few millimetres from its source. The speeds at which the flows became completely turbulent in this sense are shown as circles, ◎ , in fig. 3.

(Taylor's figure 3 is reproduced as Figure 6.)

Fig. 5. Schematic representation of Taylor's color band which described the general type of motion found analytically by Dean for laminar flow.

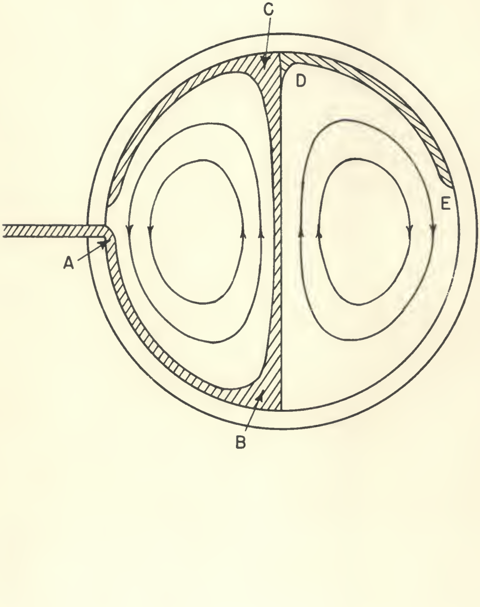
C
D
E
A
B

Further,

> Inspection of fig. 3 shows that Mr. White's conclusion is amply verified in experiments with colour bands. The flow was completely turbulent on entering the helix. This was demonstrated by passing the water first through a straight glass tube containing a 1/2-mm. hole of the same type as that in the glass helix.
>
> At approximately the speed indicated by Reynolds' criterion, $dv\rho/\mu = 2020$, the flow became turbulent in the straight pipe. It then entered the helix in this state but after passing through only one coil in the case of glass helix No. 1, or 2 1/2 coils in the case of helix No. 2, it had become steady again. This steadiness persisted up to a value $dv\rho/\mu = 5830$ in the case of helix No. 1, i.e., up to 2.8 times the speed at which turbulence persists in a straight pipe. It will be noticed in fig. 3 that Mr. White's measurements correspond far more closely with the speed at which the flow first appears completely turbulent than with the speed at which it first begins to fluctuate. This might be expected because a fluctuation which does not cause the colour band to become diffused is not likely to cause any considerable increase in resistance.

Thus White's reasoning was justified in a direct manner.

3. The Electric Double Layer

Anderson gave a rather complete account of the underlying principles of the electric double layer; a brief outline of this is given here.

From studies of colloids it is known that, at a solid-liquid interface, the solid surface becomes charged. These charges are supplied by the liquid. Since there is

Fig. 6. Reproduction of Taylor's fig. 3. White's values of the minimum critical Reynolds number are indicated by the curve + .

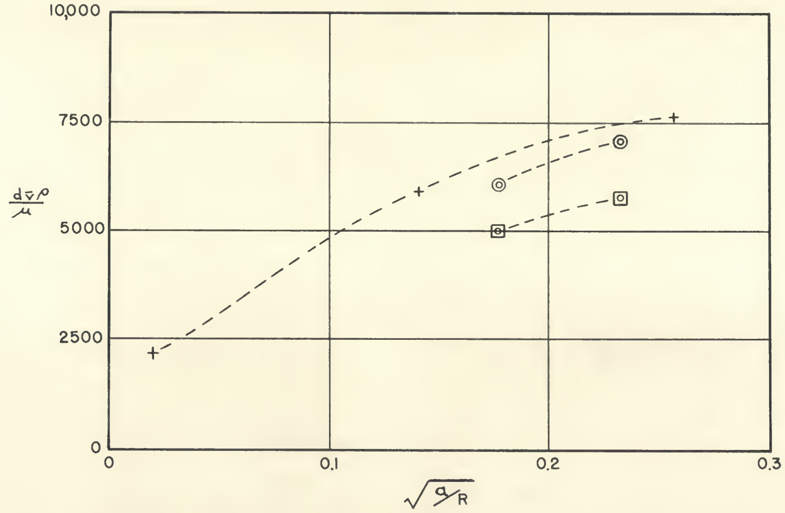
10,000
7500
5000
2500
0
$\frac{d\bar{v}\rho}{\mu}$
0
0.1
0.2
0.3
$\sqrt{a/R}$

a charge on the interface, there must also be an equal and opposite layer of charge adjacent to the interface. These charged layers are called the electric double layer. Gouy(8) and Chapman(9) considered the double layer to be ions attached to the wall and an equivalent ionic charge of opposite sign distributed in the solution near the interface.

The charge on the wall is treated as a uniform surface charge. The space charge in the solution is due to the unequal distribution of ions, assumed to have no physical size. The solvent is considered as a continuous medium entering the problem only through its dielectric constant.

Assuming an infinite flat wall, the differential equation of the potential is

$$\frac{d^2\zeta}{dx^2} = -\frac{4\pi}{\epsilon}\sum Z_i e n_{io} \exp\left(-Z_i e \zeta/kT\right) \qquad (1)$$

where	ζ	is the potential (having a value of at the wall),
	n_i	is the number density of the i^{th} ion species (having a value of n_{io} at the wall),
	Z_i	is the valence,
	ϵ	is the dielectric constant,
	e	is the electronic charge,
	k	is Boltzmann's constant,
and	T	is the temperature of the solution.

The boundary conditions are

$$\zeta = 0 \;, \quad \frac{d\zeta}{dx} = 0 \qquad \text{for} \quad x \rightarrow \infty \tag{2}$$

where X is the distance from the wall.

Letting $$X^2 = \frac{4\pi e^2 \sum_i n_{io} Z_i^2}{\epsilon k T} \tag{3}$$

and assuming $Ze\,\zeta/kT$ to be small, the solution is

$$X x = \ln\left(\frac{\zeta_o}{\zeta}\right)$$

or

$$\zeta = \zeta_o e^{-Xx} \tag{4}$$

showing that ζ drops by a factor of e^{-1} in the distance $1/X$. This value is called the thickness of the double layer or Debye length.

4. Streaming Potential

The flow of the fluid, i.e., the solvent, sweeps out ions in the movable part of the double layer, developing a streaming potential between the two ends of the passage. This potential difference causes a conduction current to flow which at equilibrium is equal and opposite to the convection current.

For laminar flow in a constant area pipe caused by a pressure gradient which is constant over the cross section, analysis yields

$$\frac{dE}{dp} = \frac{\epsilon \zeta_0}{4\pi \mu \lambda} \tag{5}$$

where	E	is the potential caused by the fluid flow,
	μ	is the absolute viscosity,
	λ	is the specific conductance,
and	p	is the pressure.

Equation (1) shows that the streaming potential, for the assumptions made, is a linear function of the pressure drop along the pipe.

The convection current is given approximately by

$$i_1 = -\frac{\epsilon}{4\pi} \oint \zeta_0 \frac{dv_n}{dx}\, ds \tag{6}$$

where	v_n	is the hydrodynamic velocity along the axis of the pipe,
and	s	is the arc length.

Equation (2) shows that the convection current, and hence the streaming potential, should be sensitive to the velocity gradient at the wall. Thus a change in the streaming potential should provide a means of detecting a change in $\frac{dv_n}{dx}$.

5. Results of Anderson's Investigation

Anderson investigated the transition to turbulence in a straight pipe of circular cross section using fluctuations in the streaming potential to indicate the onset of turbulence. As in Taylor's experiment, it was found that there was a Reynolds number at which the flow first showed some instability and another higher Reynolds number at which the flow was completely turbulent.

II. THE EXPERIMENT

1. General Description

The technique developed by Anderson for detecting the onset of turbulence utilizes the very sharp fluctuations in the streaming potential which are characteristic of turbulent flow, the turbulent eddies causing changes in velocity near the wall.

2. Laboratory

The laboratory designed by Anderson specifically for the streaming potential measurements obtains very close control of temperature and humidity. The temperature variations must be low because of the strong dependence of the fluid viscosity and density on the temperature; the low humidity is necessary because of the very small electrical currents involved: 10^{-8} to 10^{-9} amps with a source leakage on the order of 50 megohms. The temperature of the room can be controlled to $\pm 0.75^{\circ}F$ over the range 40 to $70^{\circ}F$, which is a continuous variation over a 4 minute period. The humidity of the room can be held below 20% R.H. In addition, the flow system was enclosed in a Faraday cage to avoid unwanted electrical noise.

3. Apparatus

A schematic drawing of the flow apparatus is shown in Fig. 7 . The reservoirs R_1 and R_2 are 5 liter Pyrex boiling flasks. Tubes L_1 and L_2 are 6mm Pyrex tubing. A_1 and A_2 are 8mm tubes terminating in the sockets of ground glass ball joints. The tube T is the curved pipe which is a precision bore capillary tube. The diameter of T is ± 0.0002 inches. The length of T is 24 inches. The ends of T are flared into 8mm tubes which terminate in the ball portion of the ball joints. The fluid is run from R_1 to R_2 by applying gas pressure through V_1. A glass trip is provided at B to ensure turbulent flow at the entrance to T. Either S_1 or S_2 is connected to a height gage to determine the level of the fluid in the flasks to within ± 0.002 inch.

E_1 and E_2 are Ag - AgCl electrodes based on a spiral of 24 AWG platinum.

Commercially bottled nitrogen supplied the gas pressure. A schematic diagram of the pressure system is shown in Fig. 8 . A microscope mounted on a height gage was used to read the simple mercury manometer (see Fig. 9). With this system and the accurate bleed valve the pressure could be controlled to within ± 0.005 inch Hg.

Fig. 7. Schematic sketch of experimental apparatus.

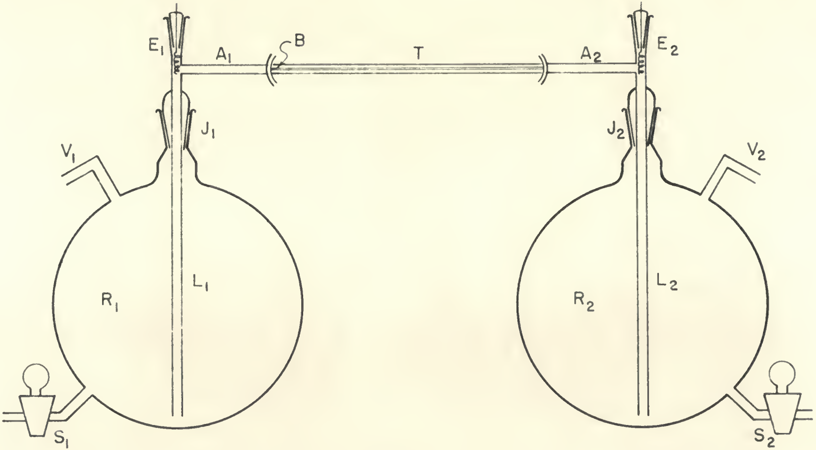
E$_1$
A$_1$
B
T
A$_2$
E$_2$
J$_1$
J$_2$
V$_1$
V$_2$
L$_1$
R$_1$
R$_2$
L$_2$
S$_1$
S$_2$

Fig. 8. A sketch of the pressure system.

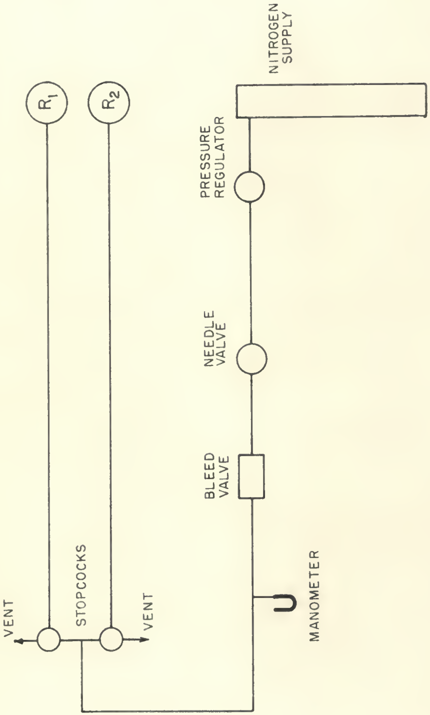
NITROGEN SUPPLY
PRESSURE REGULATOR
NEEDLE VALVE
BLEED VALVE
MANOMETER
R_1
R_2
STOPCOCKS
VENT
VENT

Fig. 9. Manometer and optical system used for the pressure measurements.

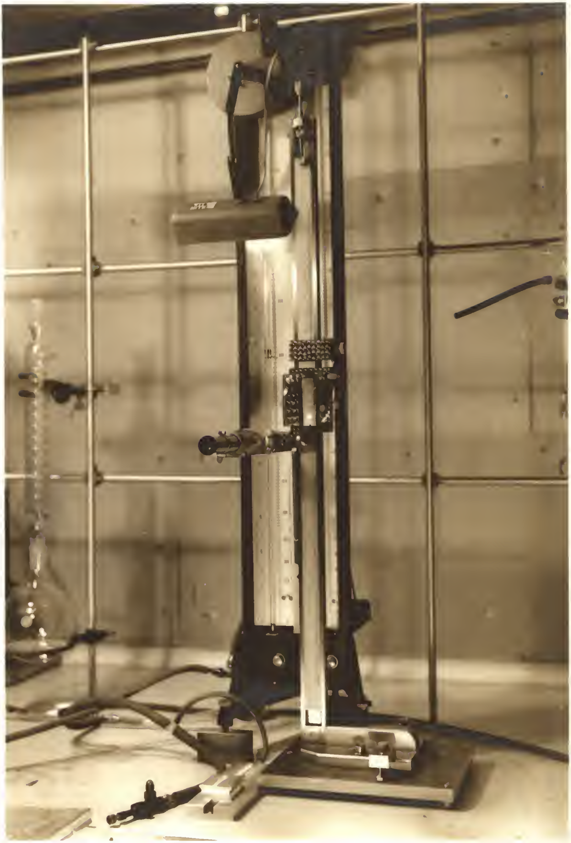

4. Curving and Measuring of the Glass Pipes

The curved pipe was formed from a precision bore Pyrex capillary tube which was curved over a precisely machined space form in a large furnace. Approximately 10 minutes in the furnace at a temperature of 740°C was required to fabricate the capillary tube. Any greater time yields an unacceptable distortion of the bore.

The diameter of the pipe in the plane of bending was measured at 3-inch intervals before and after bending using an optical comparator. The pipe rested in a tank of glycerin which possesses an index of refraction very close to that of Pyrex. By placing the bath in the temperature-controlled laboratory and adjusting the temperature, the index of refraction of the glycerin could be brought into very close coincidence with that of the Pyrex. This occurred when the outer surface of the glass was no longer visible. Tinted glycerin pumped into the tube made the inner surface visible. This system did away with the troublesome effects of refraction from the glass surfaces and permitted a precise measurement of the tube diameter.

5. Experimental Procedures

The procedure used to determine the critical Reynolds number was to measure the pressure where the turbulent fluctuations in the streaming potential first appeared. This pressure was then used to find the corresponding Reynolds number from a calibration curve obtained from mass flow measurements. The calibration curve is shown in Fig. 10 where

P is the pressure,
d is the diameter of the tube,
and l is the length of the tube.

Fig. 10. Tube calibration curve.

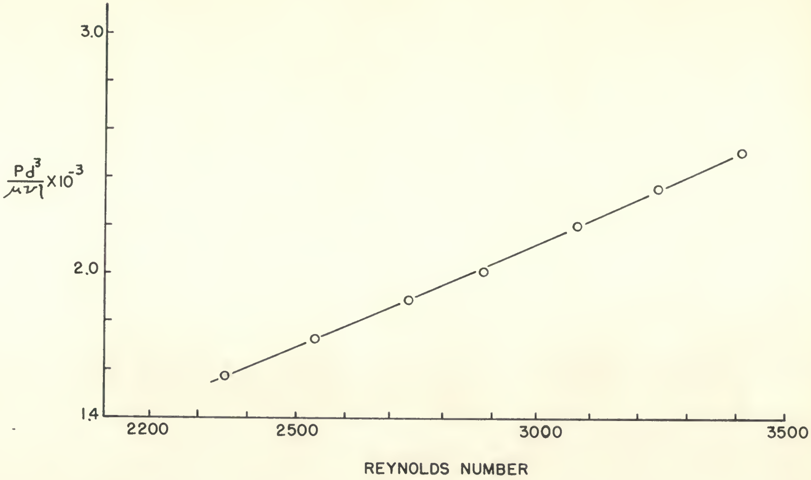
$\frac{Pd^3}{\mu \nu l} \times 10^{-3}$
3.0
2.0
1.4
2200
2500
3000
3500
REYNOLDS NUMBER

CHAPTER III

RESULTS

1. Measurements

Using the procedure previously described the critical Reynolds number was found to be 3190 with a standard deviation of 20. The critical point was found to be extremely sensitive to temperature, a variation of 1°C resulting in a change in the critical pressure of about 1 inch of Hg.

The result is plotted in Fig. 11 as the point denoted by △. This is slightly higher than the values given by White, which were obtained from mass flow measurements. This apparent difference between the two techniques is attributed to the need for longer periods of time necessary to allow for sufficient sampling of the fluctuations in the streaming potential precisely at the critical point. Such sampling periods are not possible with the present system, being limited by the size of the flasks.

Fig. 11. Critical Reynolds number vs. curvature ratio.

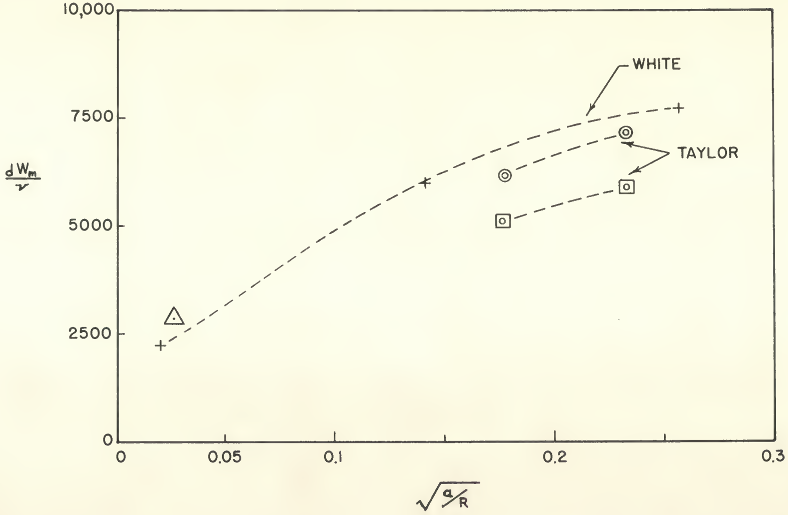
$\frac{d W_m}{\nu}$
10,000
7500
5000
2500
0
0
0.05
0.1
0.2
0.3
$\sqrt{a/R}$
WHITE
TAYLOR

APPENDIX I

The Navier-Stokes Equation for a Compressible Fluid in General Orthogonal Curvilinear Coordinates.

x_1 component:

$$\rho\Big[\frac{\partial \omega_1}{\partial t} + \frac{\omega_1}{h_1}\frac{\partial \omega_1}{\partial x_1} + \frac{\omega_2}{h_2}\frac{\partial \omega_1}{\partial x_2} + \frac{\omega_3}{h_3}\frac{\partial \omega_1}{\partial x_3}$$

$$-\omega_2\left(\frac{\omega_2}{h_2 h_1}\frac{\partial h_2}{\partial x_1} - \frac{\omega_1}{h_1 h_2}\frac{\partial h_1}{\partial x_2}\right) + \omega_3\left(\frac{\omega_1}{h_1 h_3}\frac{\partial h_1}{\partial x_3} - \frac{\omega_3}{h_3 h_1}\frac{\partial h_3}{\partial x_1}\right)\Big]$$

$$= F_1 - \frac{1}{h_1}\frac{\partial p}{\partial x_1} + \frac{1}{h_1}\frac{\partial}{\partial x_1}\left(\lambda \nabla \cdot \vec{V}\right)$$

$$+ \frac{1}{h_1 h_2 h_3}\Bigg\{\frac{\partial}{\partial x_1}\left[2\mu h_2 h_3\left(\frac{1}{h_1}\frac{\partial \omega_1}{\partial x_1} + \frac{\omega_2}{h_1 h_2}\frac{\partial h_1}{\partial x_2} + \frac{\omega_3}{h_3 h_1}\frac{\partial h_1}{\partial x_3}\right)\right]$$

$$+ \frac{\partial}{\partial x_2}\left[h_1 h_3 \mu\left(\frac{h_2}{h_1}\frac{\partial}{\partial x_1}\left(\frac{\omega_2}{h_2}\right) + \frac{h_1}{h_2}\frac{\partial}{\partial x_2}\left(\frac{\omega_1}{h_1}\right)\right)\right]$$

$$+ \frac{\partial}{\partial x_3}\left[h_1 h_2 \mu\left(\frac{h_1}{h_3}\frac{\partial}{\partial x_3}\left(\frac{\omega_1}{h_1}\right) + \frac{h_3}{h_1}\frac{\partial}{\partial x_1}\left(\frac{\omega_3}{h_3}\right)\right)\right]\Bigg\}$$

$$+ \frac{\mu}{h_1 h_2}\left\{\frac{h_2}{h_1}\frac{\partial}{\partial x_1}\left(\frac{\omega_2}{h_2}\right) + \frac{h_1}{h_2}\frac{\partial}{\partial x_2}\left(\frac{\omega_1}{h_1}\right)\right\} \cdot \frac{\partial h_1}{\partial x_2}$$

$$+ \frac{\mu}{h_1 h_3}\left\{\frac{h_1}{h_3}\frac{\partial}{\partial x_3}\left(\frac{\omega_1}{h_1}\right) + \frac{h_3}{h_1}\frac{\partial}{\partial x_1}\left(\frac{\omega_3}{h_3}\right)\right\} \cdot \frac{\partial h_1}{\partial x_3}$$

$$- \frac{2\mu}{h_1 h_2}\left\{\frac{1}{h_2}\frac{\partial \omega_2}{\partial x_2} + \frac{\omega_3}{h_2 h_3}\frac{\partial h_2}{\partial x_3} + \frac{\omega_1}{h_1 h_2}\frac{\partial h_2}{\partial x_1}\right\} \cdot \frac{\partial h_2}{\partial h_1}$$

$$- \frac{2\mu}{h_1 h_3}\left\{\frac{1}{h_3}\frac{\partial \omega_3}{\partial x_3} + \frac{\omega_1}{h_3 h_1}\frac{\partial h_3}{\partial x_1} + \frac{\omega_2}{h_2 h_3}\frac{\partial h_3}{\partial x_2}\right\} \cdot \frac{\partial h_3}{\partial x_1}$$

x_2 component:

$$\rho\left[\frac{\partial \omega_2}{\partial t} + \frac{\omega_1}{h_1}\frac{\partial \omega_2}{\partial x_1} + \frac{\omega_2}{h_2}\frac{\partial \omega_2}{\partial x_2} + \frac{\omega_3}{h_3}\frac{\partial \omega_2}{\partial x_3}\right.$$

$$\left. - \omega_3\left(\frac{\omega_3}{h_3 h_2}\frac{\partial h_3}{\partial x_2} - \frac{\omega_2}{h_2 h_3}\frac{\partial h_2}{\partial x_3}\right) + \omega_1\left(\frac{\omega_2}{h_2 h_1}\frac{\partial h_2}{\partial x_1} - \frac{\omega_1}{h_1 h_2}\frac{\partial h_1}{\partial x_2}\right)\right]$$

$$= F_2 - \frac{1}{h_2}\frac{\partial p}{\partial x_2} + \frac{1}{h_2}\frac{\partial}{\partial x_2}\left(\lambda \nabla \cdot \vec{V}\right)$$

$$+ \frac{1}{h_2 h_2 h_3}\left\{\frac{\partial}{\partial x_1}\left[h_2 h_3 \mu\left(\frac{h_2}{h_1}\frac{\partial}{\partial x_1}\left(\frac{\omega_2}{h_2}\right) + \frac{h_1}{h_2}\frac{\partial}{\partial x_2}\left(\frac{\omega_1}{h_1}\right)\right)\right]\right.$$

$$+ \frac{\partial}{\partial x_2}\left[2\mu h_3 h_1\left(\frac{1}{h_2}\frac{\partial \omega_2}{\partial x_2} + \frac{\omega_3}{h_2 h_3}\frac{\partial h_2}{\partial x_3} + \frac{\omega_1}{h_1 h_2}\frac{\partial h_2}{\partial x_1}\right)\right]$$

$$\left. + \frac{\partial}{\partial x_3}\left[h_1 h_2 \mu\left(\frac{h_3}{h_2}\frac{\partial}{\partial x_2}\left(\frac{\omega_3}{h_3}\right) + \frac{h_2}{h_3}\frac{\partial}{\partial x_3}\left(\frac{\omega_2}{h_2}\right)\right)\right]\right\}$$

$$+ \frac{\mu}{h_2 h_3}\left\{\frac{h_3}{h_2}\frac{\partial}{\partial x_2}\left(\frac{\omega_3}{h_3}\right) + \frac{h_2}{h_3}\frac{\partial}{\partial x_3}\left(\frac{\omega_2}{h_2}\right)\right\} \cdot \frac{\partial h_2}{\partial x_3}$$

$$+ \frac{\mu}{h_2 h_1}\left\{\frac{h_2}{h_1}\frac{\partial}{\partial x_1}\left(\frac{\omega_2}{h_2}\right) + \frac{h_1}{h_2}\frac{\partial}{\partial x_2}\left(\frac{\omega_1}{h_1}\right)\right\} \cdot \frac{\partial h_2}{\partial x_1}$$

$$- \frac{2\mu}{h_2 h_3}\left\{\frac{1}{h_3}\frac{\partial \omega_3}{\partial x_3} + \frac{\omega_1}{h_3 h_1}\frac{\partial h_3}{\partial x_1} + \frac{\omega_2}{h_2 h_3}\frac{\partial h_3}{\partial x_2}\right\} \cdot \frac{\partial h_3}{\partial x_2}$$

$$- \frac{2\mu}{h_2 h_1}\left\{\frac{1}{h_1}\frac{\partial \omega_1}{\partial x_1} + \frac{\omega_2}{h_1 h_2}\frac{\partial h_1}{\partial x_2} + \frac{\omega_3}{h_3 h_1}\frac{\partial h_1}{\partial x_3}\right\} \cdot \frac{\partial h_1}{\partial x_2}$$

x_3 component:

$$\rho\left[\frac{\partial w_3}{\partial t} + \frac{w_1}{h_1}\frac{\partial w_3}{\partial x_1} + \frac{w_2}{h_2}\frac{\partial w_3}{\partial x_2} + \frac{w_3}{h_3}\frac{\partial w_3}{\partial x_3}\right.$$

$$\left. - w_1\left(\frac{w_1}{h_1h_3}\frac{\partial h_1}{\partial x_3} - \frac{w_3}{h_3h_1}\frac{\partial h_3}{\partial x_1}\right) + w_2\left(\frac{w_3}{h_2h_3}\frac{\partial h_3}{\partial x_2} - \frac{w_2}{h_2h_3}\frac{\partial h_2}{\partial x_3}\right)\right]$$

$$= F_3 - \frac{1}{h_3}\frac{\partial p}{\partial x_3} + \frac{1}{h_3}\frac{\partial}{\partial x_3}\left(\lambda\nabla\cdot\vec{V}\right)$$

$$+ \frac{1}{h_1h_2h_3}\left\{\frac{\partial}{\partial x_1}\left[h_2h_3\mu\left(\frac{h_1}{h_2}\frac{\partial}{\partial x_3}\left(\frac{w_1}{h_1}\right) + \frac{h_3}{h_1}\frac{\partial}{\partial x_1}\left(\frac{w_3}{h_3}\right)\right)\right]\right.$$

$$+ \frac{\partial}{\partial x_2}\left[h_3h_1\mu\left(\frac{h_3}{h_2}\frac{\partial}{\partial x_2}\left(\frac{w_3}{h_3}\right) + \frac{h_2}{h_3}\frac{\partial}{\partial x_3}\left(\frac{w_2}{h_2}\right)\right)\right]$$

$$\left. + \frac{\partial}{\partial x_3}\left[2\mu h_1h_2\left(\frac{1}{h_3}\frac{\partial w_3}{\partial x_3} + \frac{w_1}{h_3h_1}\frac{\partial h_3}{\partial x_1} + \frac{w_2}{h_2h_3}\frac{\partial h_3}{\partial x_2}\right)\right]\right\}$$

$$+ \frac{\mu}{h_1h_3}\left\{\frac{h_1}{h_3}\frac{\partial}{\partial x_3}\left(\frac{w_1}{h_1}\right) + \frac{h_3}{h_1}\frac{\partial}{\partial x_1}\left(\frac{w_3}{h_3}\right)\right\}\cdot\frac{\partial h_3}{\partial x_1}$$

$$+ \frac{\mu}{h_3h_2}\left\{\frac{h_3}{h_2}\frac{\partial}{\partial x_2}\left(\frac{w_3}{h_2}\right) + \frac{h_2}{h_3}\frac{\partial}{\partial x_3}\left(\frac{w_2}{h_2}\right)\right\}\cdot\frac{\partial h_3}{\partial x_2}$$

$$- \frac{2\mu}{h_3h_1}\left\{\frac{1}{h_1}\frac{\partial w_1}{\partial x_1} + \frac{w_2}{h_1h_2}\frac{\partial h_1}{\partial x_2} + \frac{w_3}{h_3h_1}\frac{\partial h_1}{\partial x_3}\right\}\cdot\frac{\partial h_1}{\partial x_3}$$

$$- \frac{2\mu}{h_3h_2}\left\{\frac{1}{h_2}\frac{\partial w_2}{\partial x_2} + \frac{w_3}{h_2h_3}\frac{\partial h_2}{\partial x_3} + \frac{w_1}{h_1h_2}\frac{\partial h_2}{\partial x_1}\right\}\cdot\frac{\partial h_2}{\partial x_3}$$

BIBLIOGRAPHY

1. Anderson, R. C., An Experimental Determination of the Transition to Turbulence Using the Electric Double Layer (1965), Doctors Dissertation, University of Florida.
2. Dean, W. R., Phil. Mag. (1928) (7), 5, p. 673.
3. Goldstein, S., Modern Developments in Fluid Dynamics (1938), 1, p. 312.
4. Grindley, G. E. and Gibson, F. H., Proc. Roy. Soc. A (1908), 80, p. 114.
5. Eustice, E. L., Proc. Roy. Soc. A (1911), 85, p. 119.
6. White, C. M., Proc. Roy. Soc. A (1929), 123, p. 645.
7. Taylor, G. I., Proc. Roy. Soc. A (1929), 124, p. 243.
8. Gouy, G., J. Phys. (1910) (4), 9, p. 457; Ann. Phys. (1917) (9), 7, p. 129.
9. Chapman, D. L., Phil. Mag. (1913) (6), 25, p. 475.

BIOGRAPHICAL SKETCH

Addison Guy Hardee, Jr. was born April 7, 1938, at Mulberry, Florida. In June, 1955, he was graduated from Hillsboro High School in Tampa, Florida. From 1956 until 1960 he served as an electronics technician in the United States Coast Guard and was stationed for a time in Iceland. Following his discharge from the Coast Guard, he enrolled in the University of Florida. In December, 1964, he received the degree of Bachelor of Aerospace Engineering. In January, 1965, he enrolled in the Graduate School of the University of Florida where, until the present time, he has pursued his work toward the degree of Master of Science in Engineering.

Addison Guy Hardee, Jr. is married to the former Mildred Fe' Collar and is the father of one child. He is a member of Tau Beta Pi, Phi Kappa Phi and Phi Eta Sigma and holds a N.A.S.A. fellowship.

This thesis was prepared under the direction of the chairman of the candidate's supervisory committee and has been approved by all members of that committee. It was submitted to the Dean of the College of Engineering and to the Graduate Council, and was approved as partial fulfillment of the requirements for the degree of Master of Science in Engineering.

December, 1965

R Martin
Dean, College of Engineering

Dean, Graduate School

Supervisory Committee:

Chairman

M. H. Clarkson

B. M. Leadon

D. T. Williams

C. B. Smith

University of Florida
1853